CHEMISTRY OF MATERIALS

pubs.acs.org/cm

Article

Free Volume Manipulation and *In Situ* Oxidative Crosslinking of Amine-Functionalized Microporous Polymer Membranes

Taigyu Joo, Tae Hoon Lee, Samuel J. Kaser, Wan-Ni Wu, Sungsool Wi, Jing Ying Yeo, and Zachary P. Smith*

Cite This: *Chem. Mater.* 2024, 36, 4275−4290

Read Online

ACCESS | Metrics & More | Article Recommendations | Supporting Information

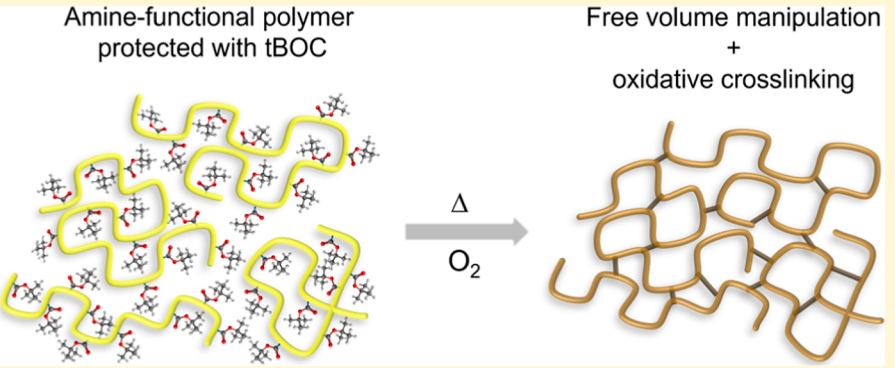

ABSTRACT: Membranes for gas separations are limited by the trade-off relationship between permeability and selectivity. In this study, we demonstrate an *in situ* thermal oxidative crosslinking strategy for amine-functionalized polymers using *tert*-butoxycarbonyl (tBOC) groups to improve separation performance. The use of labile tBOC groups offers two major benefits for inducing thermal oxidative crosslinks: (1) they trigger free radical chain reactions at more moderate temperatures, preventing polymer backbone degradation pathways that otherwise occur at elevated temperatures, and (2) they enable free volume manipulation (FVM) conditions that yield increased free volume and narrower free volume element size distribution. This thermal oxidative crosslinking strategy is demonstrated using an amine-functionalized polymer of intrinsic microporosity (PIM-NH_2). The resulting crosslinked polymer yielded up to a 22-fold increase in H_2/CH_4 selectivity while retaining 96% of H_2 permeability from pristine PIM-NH_2 films. By combining thermal oxidative crosslinks and FVM, we demonstrate an effective approach to overcome the traditional permeability−selectivity trade-off and offer a greater resistance to major performance stability issues like plasticization and physical aging, making membranes better suited for industrial applications.

1. INTRODUCTION

The increasing global demand for energy coupled with high resulting CO_2 emissions has created an urgent need for developing low-energy processes with reduced environmental footprint.[1] Given that the industrial sector is the primary contributor to energy consumption,[2] more energy-efficient industrial processes are needed. Of primary focus are chemical separations, which currently account for approximately 50% of the total energy consumed in the industrial sector, mostly through thermal separations like distillation.[3] In response, membrane technology has emerged as a promising and more energy-efficient alternative way of separating chemicals.[4] Membranes enable continuous and nonthermal separation processes without toxic mass separating agents or large spatial footprints.[4,5]

Polymeric membranes currently dominate the membrane-based gas separation market due to their processability and robust mechanical properties.[6] However, the conventional polymers used for membrane applications, such as cellulose acetate and polysulfone, are significantly limited by the trade-off relationship between permeability and selectivity, as illustrated by the classic upper bound plots.[7,8] Recently, polymers of intrinsic microporosity (PIMs) have emerged as promising contenders for next-generation membrane materials. PIMs are polymers possessing rigid backbone structures or bulky monomer units that inhibit efficient packing of polymer segments, resulting in high free volume materials when processed into a membrane.[9] The resulting high gas sorption capacity from their high free volume and high diffusion

Received: December 14, 2023
Revised: April 9, 2024
Accepted: April 10, 2024
Published: April 25, 2024

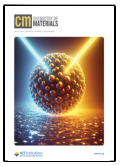

selectivity from their rigid backbones are features that have helped to redefine the upper bounds in 2015 and 2019, showing promise of PIM materials as gas separation membranes.[10−12]

To further enhance gas transport properties, postsynthetic modifications of existing PIM structures have been extensively investigated. PIM-1—the archetypal PIM containing a spirobisindane backbone—for example, has been modified with groups that have high CO_2 affinity like amines,[13] carboxylic acids,[14−17] thioamides,[18] and tetrazole.[19] These modifications not only enhance CO_2 sorption but also introduce secondary interactions, such as hydrogen bonds, that help maintain the stability of the polymer matrix against plasticization, a detrimental phenomenon that reduces membrane selectivity.[20] Crosslinking of PIMs has also been widely studied to enhance diffusion selectivity,[21−23] with several successful examples even surpassing the upper bounds. For instance, Song *et al.* thermally treated PIM-1 films at high temperature (*e.g.*, 350−450 °C) in a controlled oxygen environment to induce thermal oxidative crosslinks, which resulted in highly size-sieving PIM films with a representative sample achieving a CO_2/CH_4 selectivity of 70.[23] These modifications hold promising potential for creating membranes with high molecular-sieving capabilities. However, such modifications often lead to improved gas selectivity at the expense of gas permeability since the introduction of hydrogen bonds and crosslinks from postsynthetic modifications typically tend to tighten pore structures.[14,23,24]

Our group has recently developed a postsynthetic method to improve permeability−selectivity combinations, which we refer to as free volume manipulation (FVM). FVM is a solid-state deprotection strategy for PIMs that uses labile functional groups to alter physical packing structures.[25,26] The introduction of bulky functional groups like *tert*-butoxycarbonyl (tBOC) onto the polymer backbone widens intersegmental distances for solid-state membrane films, and the subsequent removal of these groups through heat treatment leaves behind an altered free volume distribution and an increased total free volume of membrane films. This method has proven to be highly effective for PIM-NH_2, resulting in a 38% increase in H_2 permeability and a 91% increase in H_2/CH_4 selectivity.[26] Hence, FVM can be used to maximize the benefits of postsynthetic modifications.

In this work, we demonstrate a novel modification strategy to integrate *in situ* thermal oxidative crosslinking with tBOC-based FVM to significantly improve the selectivity of PIM-NH_2 membranes without compromising permeability. In the presence of oxygen, radical chain reactions are initiated on the methylene group connecting the tBOC group and the polymer backbone, resulting in the formation of degradation species that can subsequently form new thermal oxidative crosslinked species. A key advantage of using tBOC is that it enables the use of the FVM strategy while simultaneously allowing the thermal oxidative reaction to proceed at much lower temperature, which slowly starts at approximately 180−200 °C, presenting much milder thermal treatment conditions compared to those of the previously explored thermal crosslinking strategies.[23,27,28] In-depth analyses of chemical structures and gas transport properties confirmed the synergistic combination of thermal oxidative crosslinks and FVM, which resulted in covalently crosslinked polymers consisting of spirobisindane backbone structures. The modified PIM-NH_2 membranes demonstrated excellent gas separation capabilities, surpassing the upper bound for several gas pairs. In addition, stability issues including physical aging and plasticization were also investigated, revealing that increasing the density of thermal oxidative crosslinks can effectively make the membrane samples less sensitive to physical aging or plasticizing gases.

2. EXPERIMENTAL SECTION

2.1. Thermal Oxidative Crosslinking. PIM-1, PIM-NH_2, and PIM-tBOC films were prepared as previously reported.[26,29] A comprehensive synthesis and casting procedure can be found in Section 1 of the Supporting Information. To conduct FVM on PIM-tBOC under various oxygen concentrations, PIM-tBOC films were placed on a Petri dish and then transferred to a tube furnace (Carbolite Gero HST 12/900, USA). The films were subsequently purged with gas mixtures containing 0−5% O_2 and balance N_2 gases at a rate of 0.5 L/min for at least 30 min. After the purging process, the gas supply was reduced to 0.1 L/min, and the furnace was heated gradually at a rate of 1 °C/min to 250 °C. This maximum temperature was maintained for 16 h, after which the sample was gradually cooled to room temperature. Several samples were also exposed for reduced treatment times. For example, the furnace was heated at a rate of 10 °C/min to 220 °C and maintained at this temperature for 10 min, heated at a rate of 5 °C/min to 250 °C and maintained at this temperature for 2 h, and then gradually cooled to room temperature. The heating procedure was modified to minimize tBOC deprotection at lower temperatures and to prevent temperature overshooting, which can rapidly evolve the deprotection products. A summary of these conditions is reported in Table S1, including the cumulative time each treatment condition remained above 200 °C, a temperature at which tBOC starts to degrade at an appreciable rate.

2.2. Characterization. Thermogravimetric analysis (TGA) was performed to monitor the FVM process under different oxygen concentrations using a TA Instruments 550 Thermogravimetric Analyzer (USA). An isothermal heating protocol identical to the method detailed in Section 2.1 was used while supplying 0−5% of the O_2 and balance N_2 gases. Prior to each experiment, the sample weight was stabilized using an isothermal hold at 40 °C for a duration of 10 min.

Attenuated total reflection Fourier transform infrared (ATR-FT-IR) spectroscopy was performed using a Bruker ALPHA Fourier transform infrared spectrometer (USA). For each polymer film, a total of 64 scans were collected at a resolution of 4 cm^{-1} within the spectral range of 400−4000 cm^{-1}. The peaks were normalized in reference to the maximum peak in each spectrum.

Elemental composition of samples was investigated by X-ray photoelectron spectroscopy (XPS, PHI VersaProbe II, ULVAC-PHI Inc., Japan) with an Al-Kα radiation source.

Solid-state nuclear magnetic resonance (SSNMR) spectroscopy was performed for naturally abundant ^{13}C and ^{15}N nuclei. Polymer film samples were cut into fine pieces using a razor blade, and these pieces were packed into Bruker 3.2 mm zirconia magic angle spinning (MAS) rotors. The ^{13}C MAS SSNMR spectra were collected at room temperature using a Bruker Avance Neo spectrometer (USA), which operates at a nominal power of 500.18 MHz and is equipped with a 3.2 mm HX solids probe. The spectra were collected by coadding 300 scans using a MAS spinning rate of 20 kHz, a relaxation delay of 3 s, and a spectral window of 225 ppm.

For ^{15}N SSNMR, the $^{1}H-^{15}N$ cross-polarization MAS NMR experiment was carried out using a 3.2 mm $^{1}H-^{13}C-^{15}N$ triple-resonance MAS DNP probe without mixing any radical molecules on a 14.1 T solid-state DNP NMR spectrometer that is operated with a Bruker Avance-III console (USA). The ^{15}N SSNMR spectrum of the PIM-NH_2 film was measured at room temperature, while all ^{15}N SSNMR spectra of PIM-NH_2-FVM films were measured at approximately 100 K to improve the signal sensitivity. This temperature was maintained by flowing a cooled N_2 gas stream to quench the motional dynamics of the polymer molecules to maximize the $^{1}H-^{15}N$ dipolar coupling strength. The $^{1}H-^{15}N$ CP mixing

https://doi.org/10.1021/acs.chemmater.3c03190
Chem. Mater. 2024, 36, 4275−4290

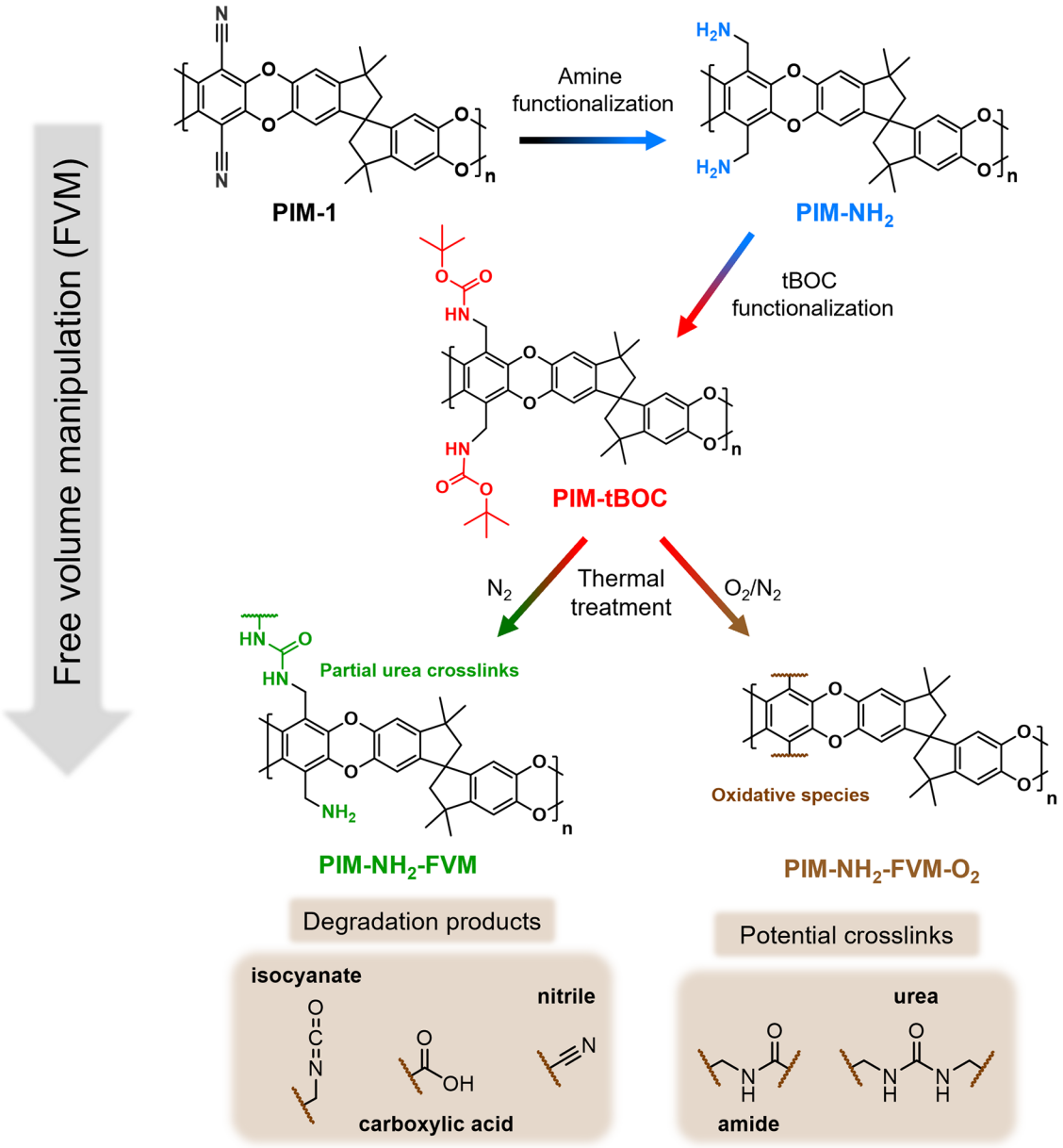

Figure 1. FVM approach for PIM-NH_2 starts with the precursor PIM-1. Light crosslinking in PIM-NH_2-FVM is represented by partial urea bond formation, and the potential species formed in the presence of oxygen are shown in the light brown boxes.

scheme was applied for 2 ms by employing a ramped (80−100%) spin-lock pulse along the ^{1}H channel at 56 kHz while simultaneously applying a rectangular spin-lock pulse of $\nu_{rf}(^{15}N)$ = 40 kHz along the ^{15}N channel. The SPINAL-64 scheme[30] with $\nu_{rf}(^1H)$ = 83 kHz was used for the ^{1}H decoupling, and the MAS spinning rate employed was 8 kHz.

2.3. Pure-Gas and Mixed-Gas Permeability Measurements. Pure-gas permeabilities of various gases (He, H_2, CH_4, N_2, O_2, CO_2, C_2H_4, and C_2H_6) were evaluated for each polymer sample by using a constant volume-variable pressure permeation testing device provided by Maxwell Robotics (USA). All samples were secured with epoxy adhesive onto brass supports to prevent leakage between the upstream and the downstream. Prior to any permeation testing, the entire apparatus was evacuated under vacuum for 8 h. When switching to a different test gas, the upstream was purged with high-pressure He, and the entire system was subjected to vacuum for 0.5−1 h after testing the lighter gases (*i.e.*, He, H_2, CH_4, N_2, O_2, and CO_2) and 6−10 h after testing heavier gases (*i.e.*, C_2H_4 and C_2H_6). All permeation tests were conducted at 35 °C with an upstream pressure of approximately 15 psia and a downstream pressure of less than 9.5 Torr.

Mixed-gas tests for 30:70, 50:50, and 70:30 CO_2/CH_4 mixture compositions were performed at 35 °C using a constant volume-variable pressure mixed-gas permeation testing device purchased from Maxwell Robotics (USA). In-depth experimental protocols can be found in a previous publication from our group.[31] Briefly, a CO_2/CH_4 gas mixture at 32 psia was supplied upstream of the film at a total flow rate of 0.24 L/min after degassing the entire system for 8 h. To verify that enough time had elapsed to reach steady state for the mixed-gas test, a pure-gas permeation test was first performed on the slower gas to estimate the time lag. For mixed-gas testing, the permeated mixture was collected in a degassed downstream chamber. This collected mixture was subsequently analyzed using a gas chromatograph (Agilent 7890B, USA).

Pure-gas permeability (P) was calculated using the following equation

https://doi.org/10.1021/acs.chemmater.3c03190
Chem. Mater. 2024, 36, 4275−4290

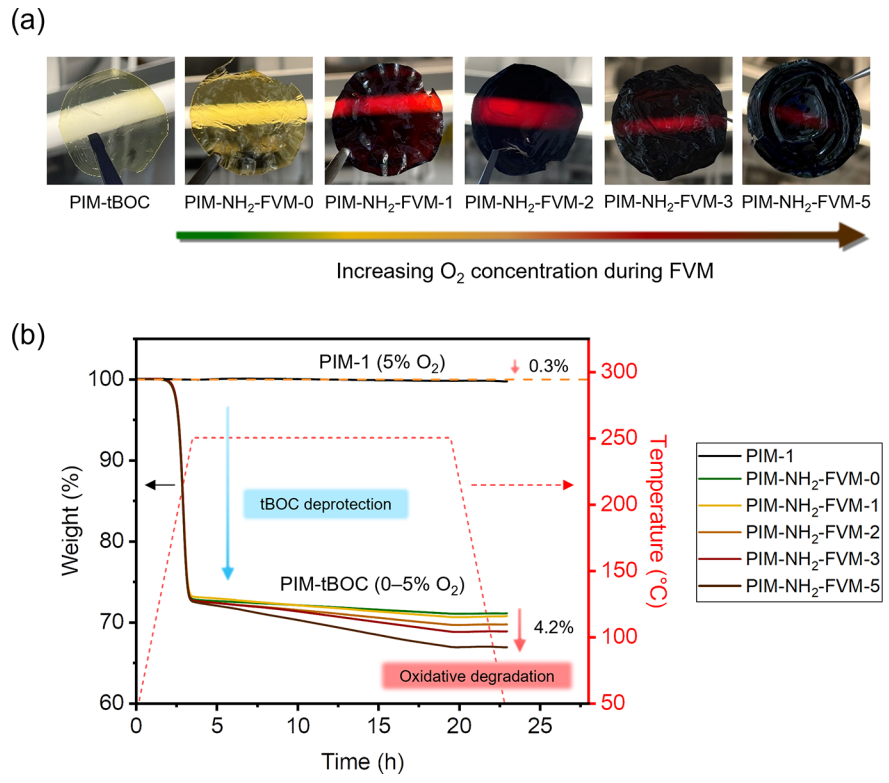

Figure 2. (a) Images of PIM-tBOC films that underwent FVM in various O_2 concentrations. The images are taken with laboratory lighting in the background to highlight the color change. (b) TGA scans of PIM-tBOC films subjected to a thermal treatment replicating the FVM process under various O_2 concentrations. Note that the sample nomenclatures in the legend correspond to the posttreatment nomenclatures. The red dotted line shows the temperature during the TGA scans (right *y*-axis). An analogous TGA scan of PIM-1 at 5% O_2 concentration is shown in black, and the dotted pale orange line represents 100 wt %.

$$P = \frac{V_d l}{\Delta p A R T}\left[\left(\frac{dp_2}{dt}\right)_{ss} - \left(\frac{dp_2}{dt}\right)_{leak}\right] \quad (1)$$

where V_d is the downstream volume, l is the film thickness, Δp is the average pressure difference between upstream and downstream, A is the active area of the films, $\left(\frac{dp_2}{dt}\right)_{ss}$ is the downstream pressure change at steady state, and $\left(\frac{dp_2}{dt}\right)_{leak}$ is the leak rate measured at the beginning of the permeation test. Mixed-gas permeability was calculated using the following equation

$$P_i = \frac{V_d l y_i}{(x_i p_1 - y_i p_2) A R T}\left[\left(\frac{dp_2}{dt}\right)_{ss} - \left(\frac{dp_2}{dt}\right)_{leak}\right] \quad (2)$$

where p_1 is the average upstream pressure, p_2 is the average downstream pressure, and y_i and x_i are the mole fractions of gas i in the downstream and the upstream, respectively. Gas selectivity ($\alpha_{i,j}$) was calculated by taking the ratio of the pure-gas and mixed-gas permeability of the more permeable gas, i, to that of the less permeable gas, j

$$\alpha_{i,j} = \frac{P_i}{P_j} \quad (3)$$

3. RESULTS AND DISCUSSION

3.1. Characterizations of Crosslinked Membrane Films. A solid-state synthetic strategy previously reported in the earlier studies[26,29] was used to incorporate tBOC groups into PIM-1 membrane films. The nitrile groups on PIM-1 were first reduced to primary amines using a borane dimethyl sulfide complex, and then, the amines were subsequently protected with tBOC groups to yield PIM-tBOC films, as shown in Figure 1. The formed PIM-tBOC films then underwent a thermal treatment process at a temperature of 250 °C for 16 h under gas mixtures containing 0−5% O_2 and balance N_2 gases to induce FVM. The samples will be denoted as PIM-NH_2-FVM-*x*, with *x* referring to the concentration of O_2 during FVM (*e.g.*, PIM-NH_2-FVM-3 for 3% O_2). Following this FVM process, the initially yellow and transparent PIM-tBOC films transitioned to a dark brown color, as depicted in Figure 2a. Increase in the oxygen concentration during the FVM process resulted in a correspondingly darker film color. As depicted in Figure 1, performing the FVM process in an inert N_2 atmosphere resulted in PIM-NH_2 films with light urea crosslinks, matching previous findings from our group.[26,29] However, the incorporation of a small amount of oxygen during the thermal treatment resulted in new thermal oxidative crosslinks, as will be discussed in the following sections. It is noted that industrially relevant asymmetric membranes, such as hollow fiber membranes, can be fabricated using the same synthesis protocol. For example, PIM-1 can be processed into hollow fibers, which then could be reduced into PIM-NH_2, functionalized with tBOC groups, and subjected to thermal treatment to yield free volume manipulated hollow fibers.

The TGA scans shown in Figure 2b illustrate the mass loss of PIM-tBOC films that are thermally treated at 250 °C for 16 h in various O_2 concentrations. For comparison, an analogous TGA scan of PIM-1 at a 5% O_2 concentration is also shown. The early hours of the FVM process were characterized by a considerable loss of mass due to the deprotection of the tBOC

https://doi.org/10.1021/acs.chemmater.3c03190
Chem. Mater. 2024, 36, 4275−4290

group, losing about 27.4% of the total mass. The theoretical mass loss for full deprotection is 29.9%, suggesting that the PIM-NH_2 film was effectively protected with tBOC at 91.6% conversion. In contrast to the PIM-NH_2-FVM-0 film, which only lost 1.8% mass after prior deprotection, the films treated in the presence of oxygen lost additional mass, with the rate of mass loss increasing with higher O_2 concentrations. After the complete deprotection of the tBOC group, the film exposed to 5% O_2 lost an additional 4.2% mass compared to the film subjected to pure N_2. In contrast, PIM-1 did not show significant mass loss throughout the entire thermal treatment process, losing only 0.3% mass, which is near the resolution of TGA. The continued and significant mass reductions following the tBOC deprotection indicate that the incorporation of tBOC groups within the polymer matrix triggers additional reactions that are particularly sensitive to the oxygen content.

ATR-FT-IR spectroscopy was used to identify potential new functional groups formed during FVM at different O_2 concentrations. As shown in Figure 3, the fresh PIM-NH_2 film without FVM displayed a spectrum consistent with previously published results.[13,26] Following FVM of PIM-NH_2 in N_2 (*i.e.*, PIM-NH_2-FVM-0), an additional peak at 1680 cm^{-1} appeared, which is associated with the carbonyl in urea crosslinks.[26] The introduction of oxygen during FVM resulted in four notable changes. First, the carbonyl peak gradually increased and broadened, shifting the peak to 1720 cm^{-1} along with introduction of additional peaks at 1774 and 1844 cm^{-1}. These changes are attributed to the formation of new carbonyl-containing species during the thermal oxidative crosslinking process, which could include species like carboxylic acids, amide, urea, and anhydride, which will be discussed later.[14,26,32] In particular, the peak at 1720 cm^{-1} aligns well with the carboxylic acid peak identified for PIM-COOH films.[14] Second, a broad and convoluted oxidation peak associated with C−O emerged in the range of 1100−1210 cm^{-1}. This finding further suggests the formation of new species that contain C−O moieties, such as anhydride and carboxylic acids. Third, a broad peak centered at approximately 2255 cm^{-1} appeared in the presence of oxygen. As will be discussed later in Section 3.2, this peak is attributed to the formation of nitrile functionality from the dehydration of primary amides[33] as well as the formation of isocyanate byproducts from the irreversible degradation of urea crosslinks in the presence of oxygen. Lastly, the intensity of the peak corresponding to the N−H band at approximately 820 cm^{-1} decreased significantly in the presence of oxygen. Degradation of primary amines in the presence of oxygen, including the formation of secondary amines, can reduce this feature, as can be gleaned by comparing spectra for PIM-NH_2, which features a primary amine, and PIM-tBOC, which contains a secondary amine. Hence, we believe this reduction is a result of primary amines undergoing thermal oxidative reaction pathways to form new crosslinks, such as amides and urea crosslinks, and to form degradation products, such as isocyanates, carboxylic acids, and nitrile groups.

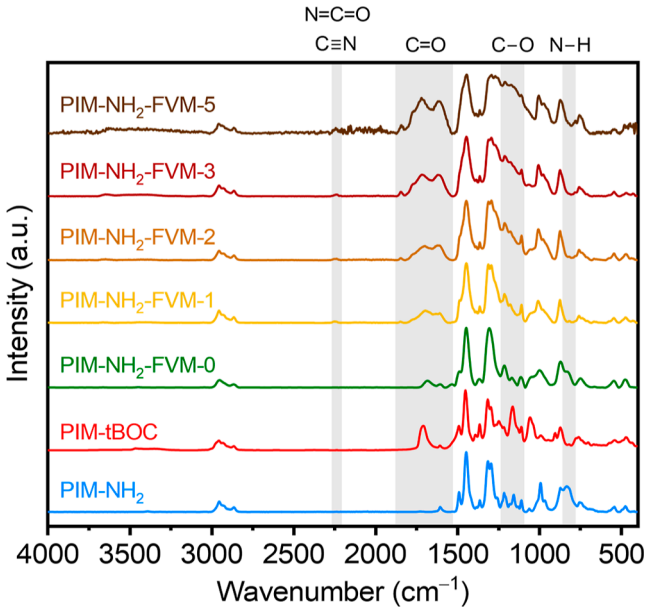

Figure 3. ATR-FT-IR spectra of PIM-NH_2, PIM-tBOC, and the free volume manipulated derivatives treated in various O_2 concentrations.

The potential chemical changes for the PIM-NH_2-FVM samples treated in various O_2 concentrations have been further explored using XPS. The high-resolution C 1s XPS spectra for PIM-NH_2 and the films exposed to 0, 1, and 3% O_2 during the FVM process are depicted in Figure 4, and the spectra for PIM-tBOC, PIM-NH_2-FVM-2, and PIM-NH_2-FVM-5 are available in Figure S4. As shown in Figure 4, the C 1s high-resolution spectrum of PIM-NH_2 revealed two primary peaks that represent the C−C bond at 284.7 eV and C−O and C−N bonds at 286.5 eV. Upon FVM of PIM-NH_2 in N_2, two additional peaks at 288.7 eV (N−C═O) and 287.7 eV (C═O) appeared, which are attributed to the formation of urea crosslinks.[34] The introduction of oxygen during FVM resulted in increases in both the C═O and N−C═O peaks, indicative of the formation of new carbonyl-containing oxidative species. The C═O peak had a particularly large increase from 0.7 to 17.3% for PIM-NH_2-FVM-3. This finding corroborates the FT-IR data and suggests the potential formation of species containing carbonyl groups, such as carboxylic acid, amide, and urea, in the presence of oxygen.

The chemical differences among PIM-NH_2 films and the free volume manipulated derivatives in various O_2 concentrations were further examined by using MAS solid-state ^{13}C NMR and ^{15}N NMR spectroscopy. As shown in Figure 5a, the ^{13}C NMR spectra for PIM-NH_2 and PIM-NH_2-FVM-0 were consistent with previously reported finding,[26] in which PIM-NH_2-FVM-0 revealed a new peak at 158 ppm corresponding to urea crosslinks. Similarly, the ^{15}N NMR spectra presented in Figure 5c showed a new peak attributed to the urea crosslinks at 78 ppm following FVM in addition to the primary amine peak at 27 ppm.[35] However, the incorporation of oxygen during FVM resulted in several changes in the chemical structure. First, the primary amine peak in ^{15}N NMR spectra disappeared, and the peaks corresponding to urea crosslinks decreased in the presence of oxygen (blue shades in Figure 5c). This finding suggests that all primary amines either degraded or reacted to form different products, while the formation of urea crosslinks was smaller in the presence of oxygen. Additionally, the urea crosslink peak at 158 ppm in ^{13}C NMR spectra broadened to 155−170 ppm, and a new minor peak at 183.5 ppm associated with aromatic aldehyde appeared in the presence of oxygen (orange shades in Figure 5b). Similarly, a new broad peak ranging from 94 to 184 ppm in ^{15}N NMR spectra emerged in the presence of oxygen (orange shade in Figure 5c). We attribute changes in chemical shifts to the formation of new thermal oxidative species, corroborating

https://doi.org/10.1021/acs.chemmater.3c03190
Chem. Mater. 2024, 36, 4275−4290

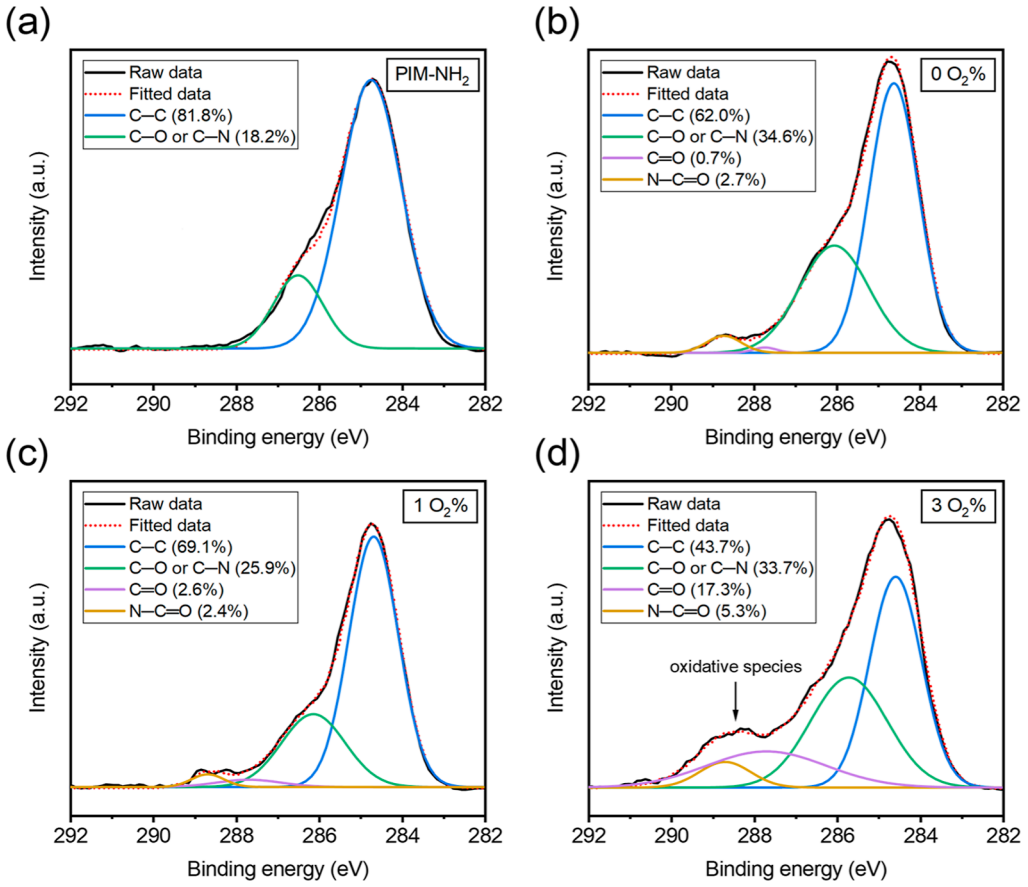

Figure 4. High-resolution C 1s XPS spectra of PIM-NH_2 and the free volume manipulated derivatives in various O_2 concentrations.

the observations in the FT-IR and XPS spectra. Moreover, the changes in line broadening of these peaks are attributed to the decrease in the flexibility of polymer chains as the extent of crosslink increases. Lastly, we observed decreases in peak intensity associated with the aromatic carbons adjacent to the dioxane moieties of the backbone as well as the methylene carbons bridging the pendant groups (gray shades in Figure 5a). These findings further suggest that the pendant groups undergo chemical changes to different species, as evidenced by the ^{15}N NMR spectra. A more detailed discussion on the formation of new chemical species is discussed in the following section.

3.2. Potential Reaction Pathways for Thermal Oxidative Crosslinks. Thermal oxidative degradation of polymers involves complex mechanisms due to the generation of highly reactive species that yield multiple reaction products.[36] Generally, the process of thermal oxidative crosslinking at high temperatures involves a series of radical-mediated reactions.[36,37] The process starts with the generation of free radical intermediates, resulting from polymer degradation. Oxygen molecules can then react with the free radical intermediates to form peroxy radicals (ROO•), which can then propagate further by abstracting a hydrogen atom from nearby side groups followed by decomposition reactions to create new radicals (RO• and •OH).[37] This pathway initiates additional free radical chain reactions that will persist until two radicals combine to terminate the radical chain reaction. It is worth noting that these reactions can result in chain scission, and the combination of two radical sites on two different chains may generate crosslinks.[37] This type of oxidative degradation mechanism has been used to explain thermal oxidative degradation for many polymers,[38−40] including the thermal oxidative crosslink study of PIM-1 by Song *et al.*[23] However, PIM-1 is known to be thermally stable up to 350 °C in air,[41] and our TGA of PIM-1 presented in Figure 2b exhibited no indication of thermal oxidative degradation before this temperature. This baseline temperature stability of the native polymer suggests that 250 °C is inadequate to trigger the thermal oxidative crosslinking pathway documented by Song *et al.* for PIM-1.[23] Thus, we hypothesize that PIM-tBOC films undergo a different thermal oxidation degradation pathway enabled by solid-state deprotection.

To elucidate the degradation pathway at a milder temperature, TGA of a PIM-NH_2 film under 5% O_2 was performed, as shown in Figure S8a. This analysis demonstrates that PIM-NH_2, much like PIM-tBOC, undergoes significant mass loss when exposed to oxygen. Furthermore, chemical characterization of PIM-NH_2 films thermally treated in an oxygen-rich environment (Figure S8b,c) highlight degradation products similar to those observed in PIM-tBOC films. More specifically, similar oxidation species were detected in the ATR-FT-IR spectrum for both samples, and the methylene group at 34 ppm in the ^{13}C NMR spectrum was notably absent for the PIM-NH_2 film as observed for PIM-tBOC films. Based on these findings, we propose that the conversion of nitrile groups to alkyl amines significantly reduces the temperature threshold for thermal oxidative degradation. Therefore, this chemical modification potentially allows crosslinking pathways, which will be discussed in detail later, to proceed at more

https://doi.org/10.1021/acs.chemmater.3c03190
Chem. Mater. 2024, 36, 4275−4290

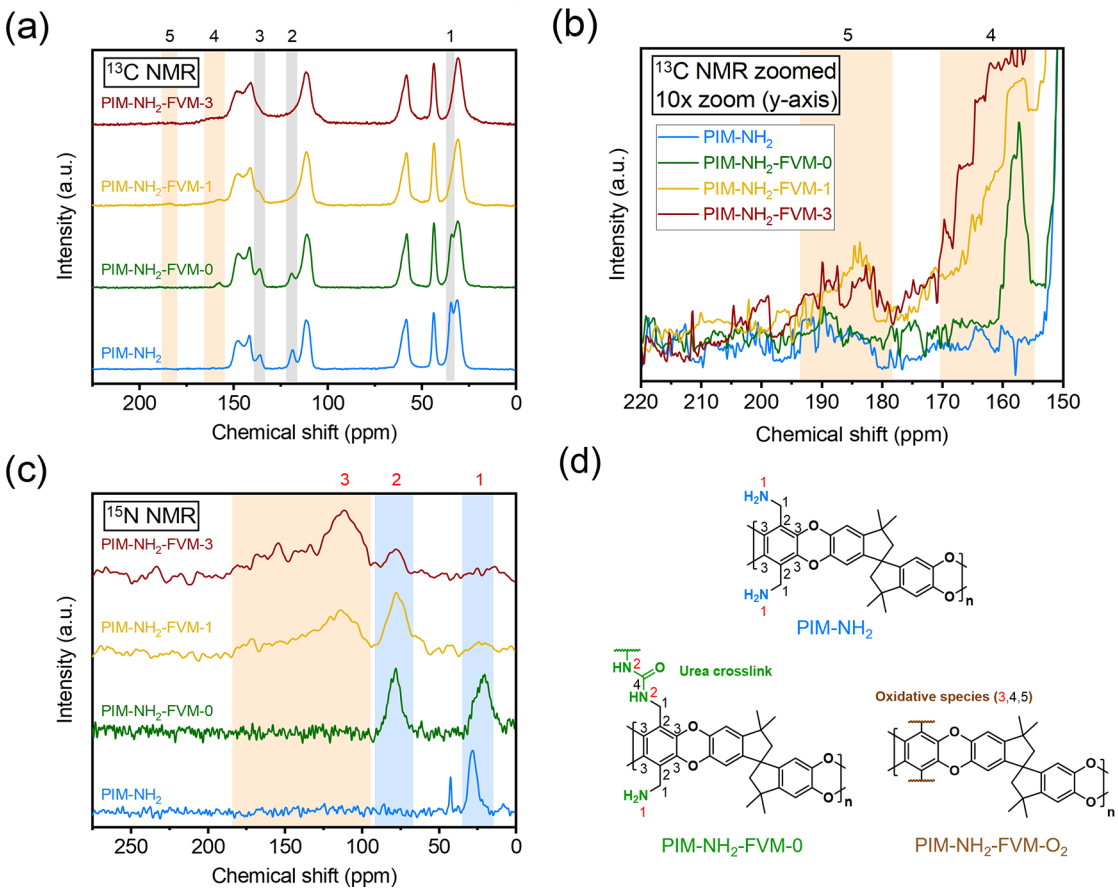

Figure 5. Solid-state (a) ^{13}C NMR, (b) zoomed-in scale of ^{13}C NMR, and (c) ^{15}N NMR spectra for the PIM-NH$_2$ film and the free volume manipulated derivatives in various O_2 concentrations. The *y*-axis in (b) is zoomed in by a factor of 10 with all spectra superimposed for clarity. The peak assignments are shown at the top of each plot. The chemical structures of PIM-NH$_2$ and PIM-NH$_2$-FVM-0 highlighting assigned peaks are shown in (d), with carbon atoms and nitrogen atoms distinguished by black and red colors, respectively. Chemical structures corresponding to the peak assignments of the oxidative species are detailed in Table S7.

Scheme 1. Potential Reaction Pathways for Primary Amine Degradation in the Presence of Oxygen[33,47]

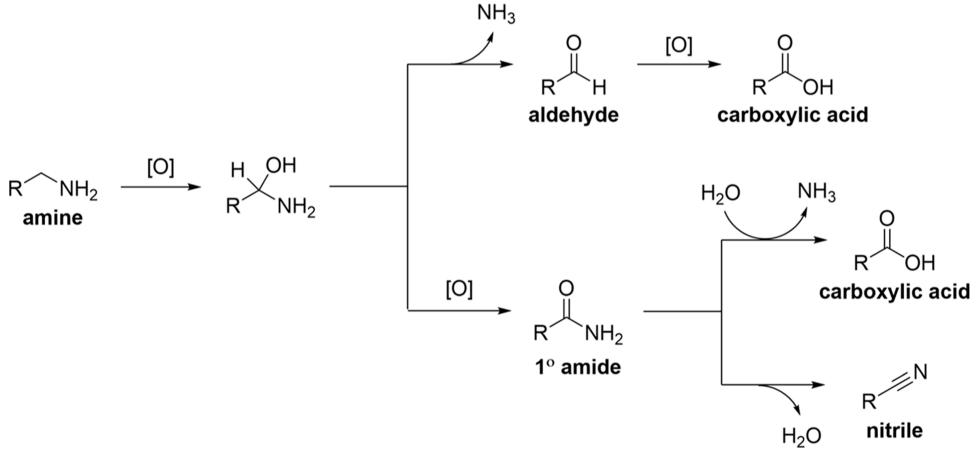

moderate temperatures compared to that of other thermal oxidative crosslinking techniques.[23,27,28] In this way, this strategy could enable enhanced performance and stability of PIM materials through lower-temperature crosslinking reactions, providing a means to modify the polymer matrix without introducing other degradation pathways that occur at higher temperatures. Thus, lower temperature treatment conditions could enable access to more relevant membrane manufacturing techniques and commercial deployment.

Table S7 summarizes the potential products formed based on the chemical characterization efforts in Section 3.1 along with a summary of supporting experimental evidence. Scheme S1 in the Supporting Information outlines the potential tBOC deprotection pathway under inert conditions, as documented in the previous FVM work.[26] In short, tBOC can degrade into

https://doi.org/10.1021/acs.chemmater.3c03190
Chem. Mater. 2024, 36, 4275−4290

Scheme 2. Potential Reaction Pathways for New Crosslinks Involving Carboxylic Acid, Isocyanate, and Amine[48−50]

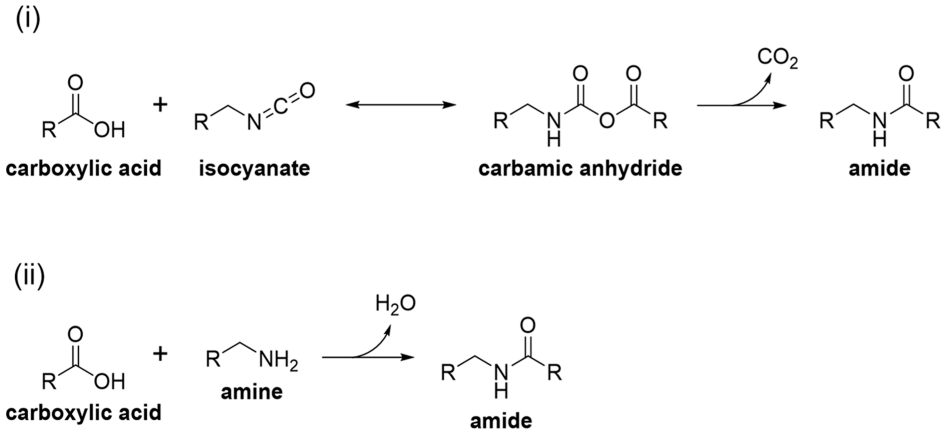

Scheme 3. Potential Reaction Pathways for Amide Crosslink Degradation in the Presence of Oxygen[43,44a]

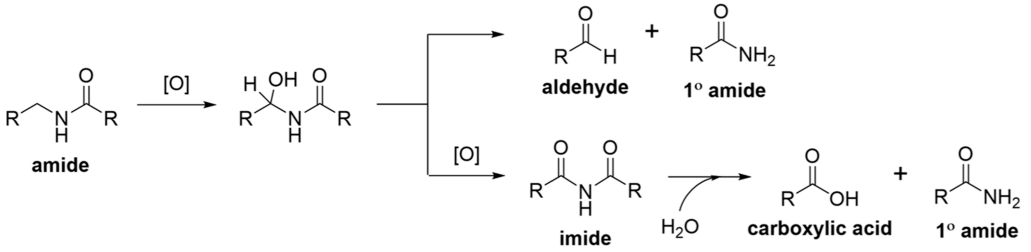

[a]Resulting primary amide and aldehyde can continue *via* the pathways shown in Scheme 1.

a primary amine group, in which isobutylene and CO_2 are byproducts. Alternatively, urea crosslinks can form due to the nucleophilic attack on either an isocyanate or a carbamic acid intermediate by a nearby deprotected amine group.[26,42] When oxygen is introduced, the deprotected primary amines can slowly undergo thermal oxidative degradation to form carboxylic acids and nitrile groups, as illustrated in Scheme 1. In polyamide oxidative degradation studies, it is commonly shown that oxidation is propagated by hydrogen abstraction on *N*-methylene.[43−45] Extending this rationale, we hypothesize that a similar oxidation mechanism can be propagated for the methylene groups adjacent to the primary amines. If so, this reaction pathway can form an aldehyde intermediate upon the loss of ammonia or a primary amide from further oxidation. The formation of an aldehyde is corroborated by the ^{13}C NMR spectra in Figure 5b, where we observe a minor peak at 183.5 ppm. We suspect that aldehyde is a minor unreacted byproduct since it would likely further oxidize to carboxylic acid in the presence of oxygen as shown in Scheme 1.[46] As for primary amides, they can be dehydrated to form a nitrile group, as observed by a minor peak at 2235 cm^{-1} in the FT-IR spectra of PIM-NH_2 treated in 5% O_2 (Figure S8b), or hydrolyzed into carboxylic acid by water byproducts.[33]

Given the potential formation of carboxylic acids from amine degradation, it opens reaction pathways for new types of crosslinks. Two potential crosslinking reaction pathways that may form from carboxylic acids are shown in Scheme 2. The first pathway involves isocyanates, which are formed as an intermediate during tBOC deprotection. Isocyanates are known to readily react with nearby alcohols and amines.[48] Hence, in addition to forming urea crosslinks as shown in Scheme S1, the nucleophilic attack of carboxylic acid on isocyanate can form carbamic anhydride, which can then further decompose to amides with CO_2 as a byproduct. The second pathway involves amines from a nearby deprotected unit. Carboxylic acids can undergo condensation reaction with amines at high temperature,[49] in which the nucleophilic attack on the carbonyl in carboxylic acid by nearby deprotected amines can yield amide crosslinks.

Given the susceptibility of aliphatic amides to thermal oxidative degradation in the presence of oxygen due to the oxidation of the methylene group adjacent to nitrogen,[43−45] it is conceivable that the amide crosslinks formed could degrade following the reaction pathways depicted in Scheme 3. Initial oxidation of the methylene can produce unstable alcohols, which can either decompose into a primary amide and aldehyde[43] or undergo further oxidation to an imide, which can further decompose by hydrolytic cleavage.[44] It is worth noting that the amine group in the primary amide is less inclined to behave as a nucleophile and form another crosslink due to the delocalization of the electron lone pair with the carbonyl carbon.[51] As a result, the primary amide can further degrade, producing either carboxylic acid or nitrile *via* the pathways highlighted in Scheme 1. In addition to the potential degradation of amide crosslinks, the urea crosslinks formed may also undergo degradation. Urea is known to be able to reversibly break down into an isocyanate and amine at high temperatures, especially in the presence of bulky substituents like polymer chains in our case.[52] This reversibility of urea crosslinks suggests that isocyanates can be continuously regenerated and then readily react with nearby amines to form new urea crosslinks. Hence, isocyanates were not detected in the FT-IR spectrum under inert conditions (*i.e.*, PIM-NH_2-FVM-0). However, if the nearby amine is oxidized to the primary amide, it no longer acts as a nucleophile, resulting in irreversible degradation of urea crosslinks. This

https://doi.org/10.1021/acs.chemmater.3c03190
Chem. Mater. 2024, 36, 4275−4290

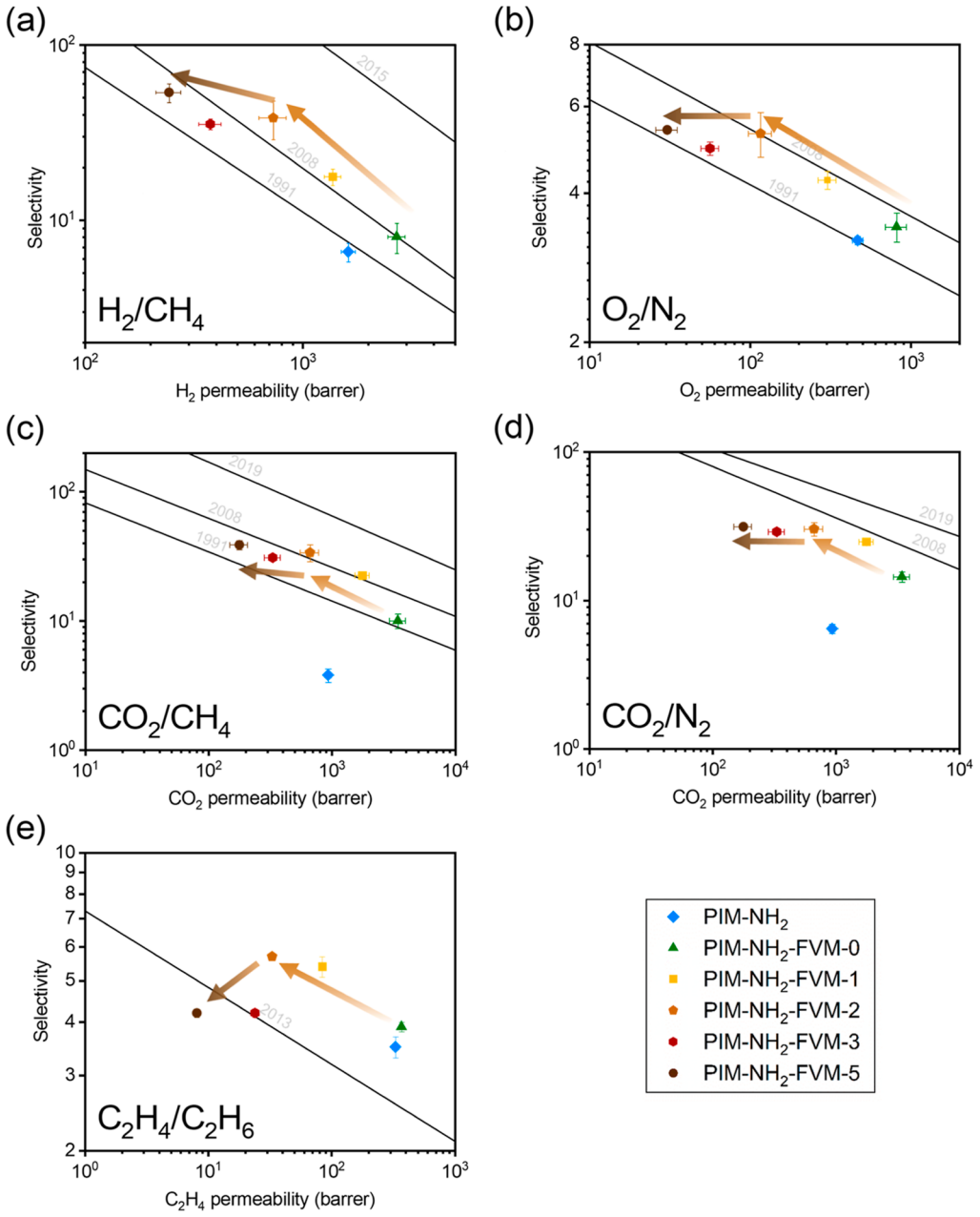

Figure 6. Permeability and selectivity for PIM-NH_2 and the FVM derivatives treated in various O_2 concentrations. The membrane films are compared against the upper bound[7,8,10,11,57] for (a) H_2/CH_4, (b) O_2/N_2, (c) CO_2/CH_4, (d) CO_2/N_2, and (e) C_2H_4/C_2H_6 gas pairs.

mechanism of nucleophilicity suppression by amine oxidation would potentially explain why the urea peaks were diminished in the SSNMR spectra (Figure 5c) when oxygen is present during FVM. We further note that hydrolysis of primary amides into carboxylic acids can result in the formation of a new amide crosslink, as illustrated in Scheme 2, whereas the dehydration of primary amide into nitrile will result in unreacted isocyanate species, which explains why we observe the broad convoluted peak at 2255 cm^{-1} in FT-IR, associated with both isocyanate and nitrile, compared to only the nitrile peak at 2235 cm^{-1} for the PIM-NH_2 film treated in oxygen (Figure S8b). These potential crosslink degradation pathways indicate that oxygen is a critical variable for tuning functionality and crosslinking.

3.3. Gas Transport Properties of Crosslinked Membrane Films. The influence of thermal oxidative crosslinks of PIM-NH_2 during FVM was investigated for gas separation performance. The gas permeation results are presented in Figure 6, and the tabulated values are shown in Tables S8 and S9. To ensure reproducibility for each FVM condition,[53] at least four independent samples from distinct FVM treatment experiments were considered for He, H_2, CH_4, N_2, O_2, and CO_2. The average values along with their standard deviations are shown in the figure. Additional permeation testing was considered for one film each for C_2H_4 and C_2H_6, and for those samples, uncertainty was estimated from propagation error analysis.

As shown in Figure 6, the changes in the concentration of the O_2 during the FVM process resulted in substantial changes to the gas separation performance, with some data points surpassing the upper bounds. In particular, for ethylene/ethane separation, which is known to be challenging due to similarities

https://doi.org/10.1021/acs.chemmater.3c03190
Chem. Mater. 2024, 36, 4275−4290

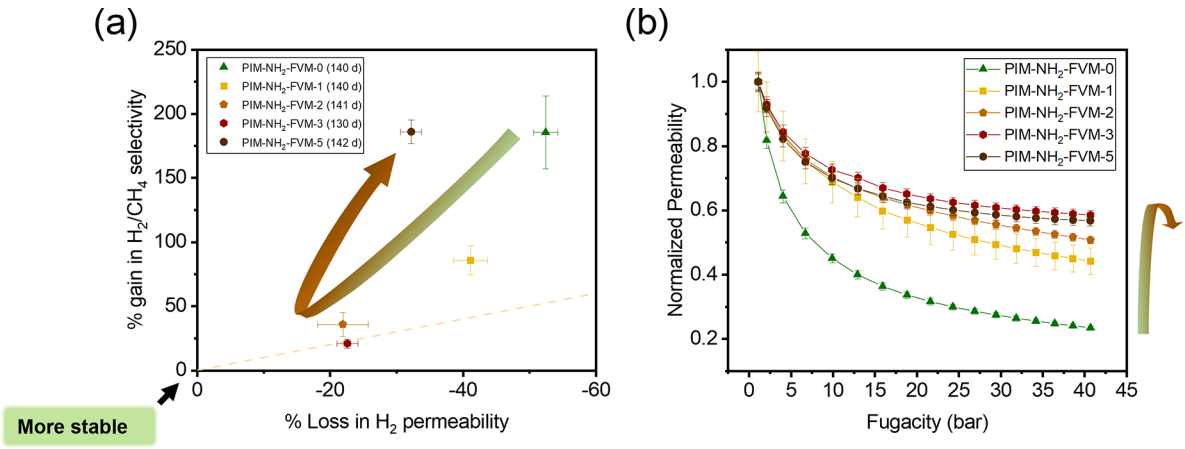

Figure 7. Comparison of (a) long-term physical aging effects on H_2/CH_4 separation for PIM-NH_2 membrane films that have undergone FVM at various O_2 concentrations and (b) normalized CO_2 permeabilities for the PIM films at various feed fugacities. The dotted yellow line in (a) is a parity line.

in the sizes and chemical properties of the gases,[6,54] a substantial selectivity increase of up to 63% was observed following the thermal oxidative crosslinking method. However, a consistent trade-off pattern was observed across all gas pairs. Increasing oxygen concentration resulted in increases in selectivity and decreases in permeability. For instance, adding a 1% O_2 concentration during FVM resulted in a 15% decrease in H_2 permeability and a 170% increase in selectivity for the H_2/CH_4 gas pair, while adding a 5% O_2 concentration resulted in an 85% decrease in permeability and a 720% increase in selectivity relative to the pristine PIM-NH_2 films. Crosslinking extent in membranes typically has a positive correlation with selectivity and a negative correlation with permeability, as we observed here. This trade-off relationship is primarily due to reduced free volume as well as restricted thermal motion of backbones for diffusional jumps.[21−23,55,56] As shown in the WAXS patterns in Figure S6 and the calculated *d*-spacing in Table S5, the average interchain distances generally decreased with the higher O_2 concentration, which indicates tighter packing structures and potentially reduced free volume. Additionally, the BET surface area calculated using CO_2 adsorption at 273 K generally decreased with increasing O_2 concentration, as shown in Table S6. The tighter packing structure may result from higher concentration of amide crosslinks since amide crosslinks have one fewer carbon compared to that of urea crosslinks, as illustrated in Figure 1. As a result of these morphological changes, the diffusivity of all gases significantly decreased with increasing O_2 concentration during FVM, and the change in diffusion selectivity was the main contributor to the selectivity increase, as shown in Figure S9. However, compared to PIM-NH_2, which did not undergo FVM, we note that certain oxidatively crosslinked samples showed improvements in both permeability and selectivity. For example, PIM-NH_2-FVM-1 had better combinations of permeability and selectivity than did PIM-NH_2 for CO_2/CH_4 separations. Therefore, controlling the O_2 content during deprotection can be used to selectively modify the polymer structure and free volume, and hence gas transport performance. In certain cases, the combined benefits of FVM and the treatment with O_2 can help to significantly improve overall transport performance.

Another consistent trend was that selectivity plateaued or slightly decreased beyond 2−3% of the O_2 concentration, whereas permeability continued to drop substantially. For instance, the O_2/N_2 selectivity was identical within measurement uncertainty despite a 75% decrease in the level of the O_2 permeability when the O_2 concentration was raised from 2 to 5%. As discussed in Section 3.2, both amide and urea crosslinks can undergo degradation by the oxidation of methylene groups. Thus, the high concentration of oxygen during FVM could result in a lower overall crosslinking degree. From our previous comparison of activation energy between PIM-NH_2 and PIM-NH_2-FVM,[29] the energy barriers were notably higher for larger gases in the PIM-NH_2-FVM sample. This resulted in enhanced selectivity despite an increased free volume, and such an effect was attributed to the crosslink network increasing the energy required for gas molecule permeation. In this case, the concomitant reduction in crosslinking and free volume can diminish gas separation performance at high O_2 concentrations, suggesting that there is an optimal oxygen concentration. Within this regime, there is balance between the formation of new thermal oxidative crosslinks and the irreversible degradation of crosslinks.

While permeability and selectivity are key performance metrics for membrane films, high free volume glassy polymers, such as the samples considered in this study, also need to be investigated for stability against physical aging. Physical aging is a slow structural relaxation process of glassy polymers moving toward an equilibrium packing state.[24] Because polymer segments are kinetically trapped in their glassy state, the gradual relaxation of polymer conformations results in a slow densification process of the polymer matrix over time, thereby reducing the free volume and changing the membrane property sets.[58] This process is especially detrimental to high free volume structures like PIMs since the physical aging rate is highly correlated to the initial free volume of polymers.[29] Figure 7a shows the comparison of selectivity gain and permeability loss with approximately 140 days of aging for the PIM-NH_2-FVM samples treated in various O_2 concentrations, and Table S11 shows the thickness of the samples presented in Figure 7a, which ranged approximately 40−60 μm. Data points closer to the origin indicate more stable membrane performance due to smaller performance changes. PIM-NH_2-FVM-0 showed a substantial 185% gain in the H_2/CH_4 selectivity after 140 days of aging, surpassing the selectivity gain of PIM-NH_2 films aged over 417 days.[29] This result further supports our

https://doi.org/10.1021/acs.chemmater.3c03190
Chem. Mater. 2024, 36, 4275−4290

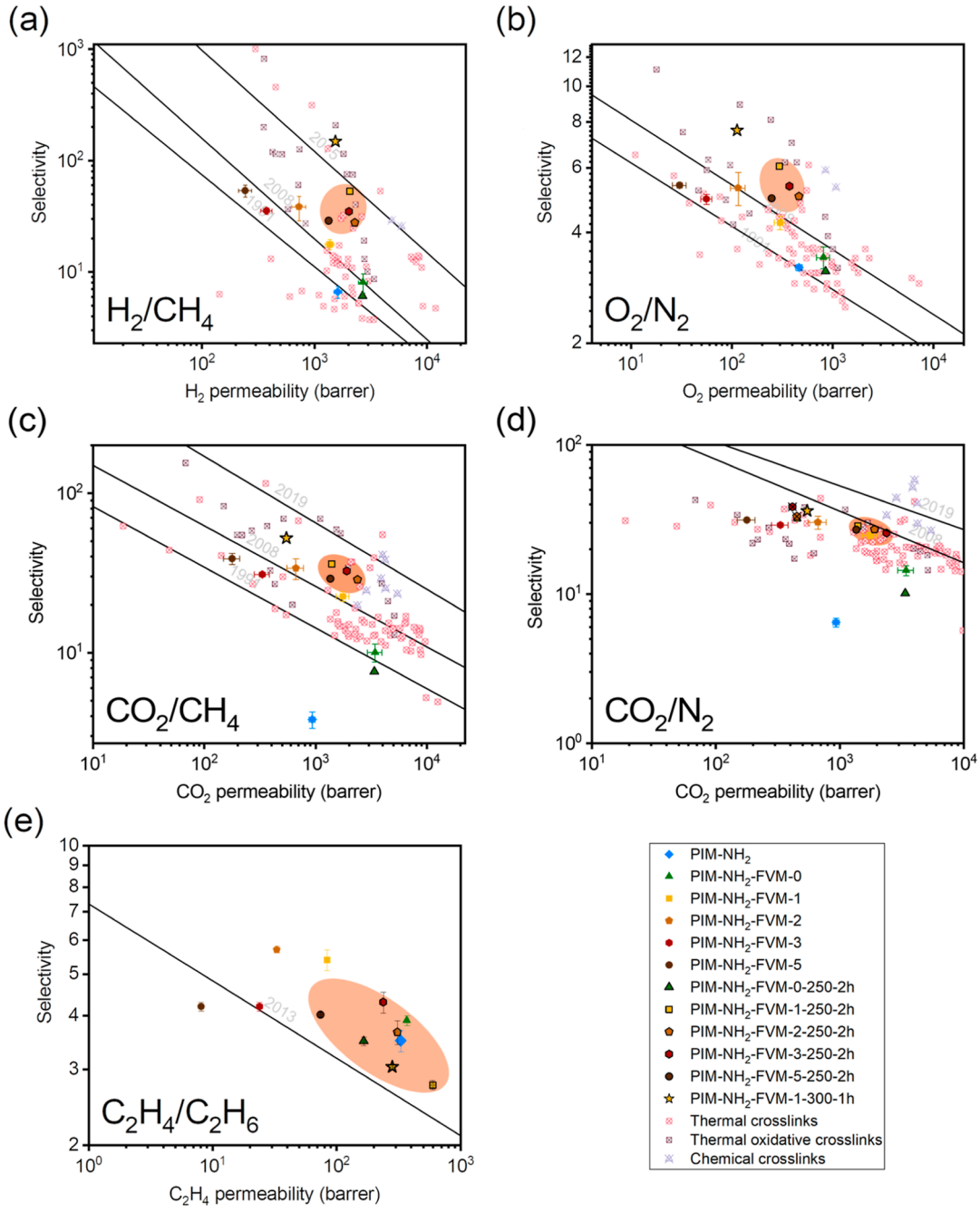

Figure 8. Permeability and selectivity for PIM-NH_2 and FVM derivatives treated in various O_2 concentrations. The membrane films are compared against the upper bounds[7,8,10,11,57] for (a) H_2/CH_4, (b) O_2/N_2, (c) CO_2/CH_4, (d) CO_2/N_2, and (e) C_2H_4/C_2H_6 gas pairs. The symbols with dark edges indicate the films that have undergone 2 h thermal treatment process, and the star symbol indicates the film that has undergone 1 h thermal treatment at 300 °C. Gas transport properties of other crosslinked PIM polymers available in literature studies are also shown for comparison.[21−23,26,63−73]

earlier finding that introducing crosslinks to PIMs substantially increases selectivity changes with aging by primarily affecting the diffusion of larger gas molecules.[29] In contrast, the membrane performance changes over 140 days became smaller with increasing O_2 concentration during FVM. As previously discussed from the WAXS patterns in Figure S6, the new thermal oxidative crosslinks potentially decrease the initial free volume and result in slower physical aging rates. Interestingly, PIM-NH_2-FVM-5 showed higher changes in both permeability and selectivity compared to that of PIM-NH_2-FVM-2 and 3. While a further investigation of free volume is required to elucidate this effect, this finding implies that long-term stability to physical aging could be compromised at higher O_2 concentrations during FVM.

Penetrant-induced plasticization is a significant challenge for the deployment of membranes for various applications in the gas processing sector. Both natural gas and biogas purification involve CO_2 removal, making CO_2/CH_4 separation an important test case for quantifying stability to plasticization.[59] Under industrially relevant pressures, condensable penetrants like CO_2 increase segmental and cooperative modes of motion in the polymer, leading to substantial losses in selectivity.[20]

https://doi.org/10.1021/acs.chemmater.3c03190
Chem. Mater. 2024, 36, 4275−4290

Effective methods to mitigate plasticization involve increasing interchain rigidity with addition of strong secondary interactions, thermal annealing, or chemical crosslinking.[20] Thus, we investigated the influence of varying the degree of thermal oxidative crosslinks on CO_2-induced plasticization of the PIM-NH_2 derivatives that have undergone FVM at various O_2 concentrations. Figure 7b depicts the normalized CO_2 permeabilities for the PIM films at various feed fugacities, and Figure S10 shows the plasticization curves on an absolute scale. As shown in Figure 7b, no sample showed a pure-gas plasticization pressure up to the tested feed fugacity of 42 bar, aligning with the previously reported study of PIM-tBOC films that underwent FVM at 250 °C in vacuum for 27 h.[31] The significant drop in permeability at low fugacity is associated with the saturation of the Langmuir sorption mode.[20] In contrast to PIM-NH_2-FVM-0, the membrane films treated with an increasing O_2 concentration showed an incrementally smaller permeability reduction with increasing feed pressure. This trend was apparent until the 5% O_2-treated sample, although normalized permeability trends for that sample were similar to those of the 3% O_2-treated sample. Upon extracting the Langmuir sorption capacity of each sample for CO_2 using the dual-mode sorption model[60] from the high-pressure CO_2 sorption experiments (as depicted in Figure S11), it was found that the Langmuir sorption capacity reduced consistently with increasing O_2 concentration during FVM, as shown in Table S12. This reduction in the concentration of the Langmuir sorption mode correlates with the shift in *d*-spacing, indicating that increasing polymer chain packing is closely tied to reductions in accessible non-equilibrium free volume. From a practical perspective, increasing crosslink density can be an effective strategy for making the membrane samples less sensitive to feed pressure, although potential compromises in sorption should also be considered.

3.4. Influence of Treatment Time in Gas Transport Properties. In Section 3.2, we discussed the possibility of new crosslink formation and their degradation in the presence of oxygen at high temperature. Since oxygen molecules are known as stable diradical molecules because their highest occupied molecular orbitals possess two unpaired electrons,[61] an oxygen-rich environment could accelerate the degradation process. Given this reaction mechanism, the oxygen concentration, crosslinking, and functional group degradation will all influence the final polymer structure. Considering that tBOC undergoes complete deprotection within roughly 2 h of the thermal treatment process as demonstrated in the TGA scans in Figure 2b, longer thermal annealing times result in increased crosslink degradation. As a result, we hypothesized that reducing the duration of thermal treatment could offer multiple advantages: (1) irreversible degradation of formed crosslinks could be minimized; (2) a decrease in thermal treatment time could lead to a smaller degree of densification, yielding higher permeabilities; (3) a higher crosslink density could result in increased selectivity values. To this end, we reduced the thermal treatment time to 2 h to observe the influence of treatment time during the thermal oxidative crosslink process. In addition to reducing the treatment time, we increased the temperature ramp rate to minimize tBOC deprotection before reaching 250 °C. Figure S12 shows the TGA scans of films that had been subjected to 2 h of the thermal treatment. These TGA scans indicate the complete deprotection of the tBOC groups within 2 h. The FT-IR scans in Figure S13 still displayed the convoluted nitrile and isocyanate peak near 2250 cm^{-1}. However, the intensity of this peak was reduced for PIM-NH_2-FVM-1-2 h. This finding suggests that oxidative degradation occurs even with the reduced thermal treatment time, but the total mass loss was lower than that of the sample treated for 16 h.

Figure 8 presents the gas transport properties of the films that have undergone a 2 h thermal treatment process (represented by symbols with dark edges) and compares their performances with the 16 h-treated samples and other crosslinked PIMs from the literature. As shown in the figure, the reduced treatment time resulted in significant increases in both permeabilities and selectivities for some gas pairs. For instance, reducing the treatment time for the 1% O_2 sample increased H_2 permeability from 1370 to 2060 barrer (a 50% increase) and the H_2/CH_4 selectivity from 18 to 53 (a 194% increase). These increases are a 27% increase in permeability and a 700% increase in selectivity compared to those of pristine PIM-NH_2 films. Thus, the reduced thermal treatment time can help maintain the free volume structure derived from removal of the bulky tBOC groups while still preserving the diffusion selective characteristics of the crosslinks. Interestingly, the film treated in 1% O_2 for 2 h had the highest selectivities for all gas pairs, unlike the 16 h-treated samples which displayed increasing selectivity with an increasing O_2 concentration. In this way, the shorter treatment time can help prevent significant irreversible degradation of formed crosslinks while still promoting the formation of new thermal oxidative crosslinks. In contrast to light gases, C_2 separation for samples with the reduced treatment time did not result in a significant improvement in transport properties relative to pristine PIM-NH_2. This finding highlights the complexity of C_2 separation, and a more comprehensive understanding will be explored in our future studies using sorption and free volume analysis. Further reducing the treatment time to 1 h while increasing the treatment temperature to 300 °C at 1% O_2 resulted in a further selectivity increase for all gas pairs (the star symbols in Figure 8). In particular, the H_2/CH_4 selectivity reached a remarkable value of 148 while maintaining a H_2 permeability of 1550 barrer. The number of variables for this treatment approach suggests that even further optimization is possible, and the investigation of the crosslinking and degradation kinetics for optimization of this thermal oxidative crosslink strategy will be the subject of our future studies.

To evaluate the membrane performance in more industrially relevant conditions, mixed-gas permeation tests using CO_2/CH_4 mixtures (30:70, 50:50, and 70:30 ratios) at 32 psia were conducted for the PIM-NH_2-FVM-1-300-1 h film that had been aged for 92 days. As shown in Figure 9 and Table S16, CO_2 permeabilities slightly decreased as the CO_2 composition increased from 30 to 70%. As discussed in Section 3.3, this finding aligns with the expected Langmuir sorption in glassy polymers when there is no substantial plasticization. In contrast to the CO_2 mixed-gas permeability results, the CH_4 mixed-gas permeability decreased with increasing CH_4 composition. This finding suggests that there is an increasing competitive sorption effect at higher CO_2 compositions since more CO_2 molecules can exclude CH_4 molecules from the polymer matrix. Such an effect has been documented for other glassy polymer membranes[31,62] and underscores the importance of evaluating mixed-gas permeation alongside pure-gas measurements. The previous study on mixed-gas permeations of PIM-NH_2 revealed that selectivities typically increase with

https://doi.org/10.1021/acs.chemmater.3c03190
Chem. Mater. 2024, 36, 4275−4290

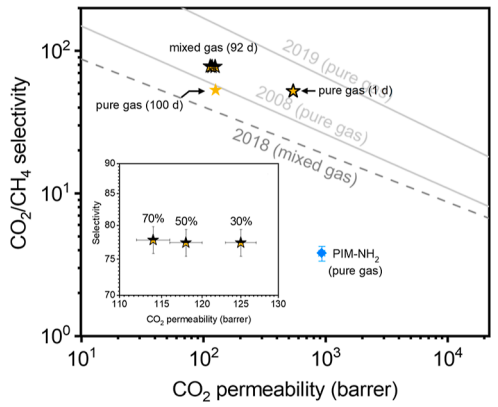

Figure 9. Mixed-gas performance (half-filled star symbols) of the PIM-NH_2-FVM-1-300-1 h film aged for 92 days. Inset corresponds to zoomed-in scale of the same plot, and the membrane films are compared against the 2008 and 2019 pure-gas as well as the 2018 mixed-gas upper bound for CO_2/CH_4 gas pairs.[5,8,11] Pure-gas data for the PIM-NH_2-FVM-1-300-1 h and PIM-NH_2 films are shown as a reference. Pure-gas performance was tested at 15 psia, and mixed-gas performance was collected at a total pressure of 32 psia at 30, 50, and 70% CO_2.

increasing CO_2 concentration,[31] which is attributed to the correlation between the competitive sorption effect and the CO_2 to CH_4 molar ratio. However, the mixed-gas selectivities remained constant within error for the PIM-NH_2-FVM-1-300-1 h film when the CO_2 composition was changed. Similarly, the mixed-gas selectivity for PIM-NH_2-FVM-1-300-1 h only increased by 45% from the pure-gas selectivity compared to a 140% increase for PIM-NH_2.[31] These findings suggest that as primary amines form new amide crosslinks during FVM, the decrease in the concentration of primary amines, which have the highest CO_2 affinity among all functional groups studied for PIM-1 derivatives,[31] is likely going to limit the competitive sorption effects compared to pristine PIM-NH_2 films. Nevertheless, PIM-NH_2-FVM-1-300-1 h (92 d) showed a mixed-gas selectivity of 77 ± 2 for the 50:50 CO_2/CH_4 mixture in comparison to the PIM-NH_2 (290 d) mixed-gas selectivity of 29 ± 2,[31] demonstrating the large diffusion selectivity benefit from the thermal oxidative crosslinks. From an application perspective, it should be noted that reaching these selectivities for CO_2/CH_4 separation with a microporous polymer is exceedingly rare for thermal crosslinking below 350 °C.

The implementation of FVM and adjusted treatment conditions resulted in a substantial improvement in both permeability and selectivity, allowing the crosslinked samples to approach or surpass the latest upper bounds. When compared against other crosslinked PIMs documented in the literature, as shown in Figure 8, the samples in this work with the shorter treatment time demonstrated an impressive balance of high permeability and selectivity, exceeding the performance of most other crosslinked PIMs. Notably, the samples in this study demonstrated high separation performance for gas pairs that heavily depend on size-sieving properties (*e.g.*, H_2/CH_4 and O_2/N_2), suggesting that the crosslinked membranes have substantially enhanced molecular-sieving capability. When comparing all data for thermal oxidative crosslinked membranes (including our data and the data from two other thermal oxidative crosslinking studies highlighted by light purple, crossed-square symbols in Figure 8[21,23]) to other crosslinking methods, it is clear that thermal oxidative crosslinking is a highly effective strategy to enhance the molecular-sieving properties of PIM structures. This unusual and highly desired enhancement of both permeability and selectivity presents a promising pathway toward optimizing the gas separation performance of various other amine-functionalized polymers, even beyond the classic PIM structure. Beyond gas separation applications, thermal oxidative crosslinking holds promise for other membrane applications, such as organic solvent nanofiltration. The formation of crosslinks can provide robust solvent resistance, while the addition of new polar functional groups can enhance the sorption of small polar organic molecules.

4. CONCLUSIONS

In this study, we demonstrated a generalizable approach to induce thermal oxidative crosslinks while simultaneously altering packing structures using the FVM strategy to enhance the molecular-sieving properties of membrane films. The reduction of the nitrile group in PIM-1 to an alkyl amine group enabled the oxidative degradation reaction to occur at more moderate temperatures compared to those of other thermal crosslinking methods in the literature, while the incorporation of tBOC as an amine-protecting group for PIM-NH_2 enabled the use of the FVM strategy. The investigation of chemical differences using FT-IR, XPS, and SSNMR indicated the formation of oxidative degradation species, such as carboxylic acids and nitrile groups, and the formation of new amide crosslinks. It was also observed that thermal oxidative degradation pathways led to irreversible degradation of existing amide and urea crosslinks, resulting in an optimal O_2 concentration for a maximum crosslink density. The pure-gas permeation and sorption results revealed significant changes in membrane transport properties with increasing O_2 oxidation treatment concentrations. In addition, the increased crosslink density provided a high resistance to physical aging as well as stability to permeability changes with increasing CO_2 feed pressure. This study discloses a mild-temperature crosslinking strategy using labile pendant groups that effectively tunes the molecular-sieving properties of amine-functionalized polymers. Applying this strategy to various polymer compositions offers the potential for significant improvements in both separation performance and long-term stability for gas separation membranes.

■ ASSOCIATED CONTENT

Supporting Information

The Supporting Information is available free of charge at https://pubs.acs.org/doi/10.1021/acs.chemmater.3c03190.

Experimental methods, gel content data, density data, wide-angle X-ray scattering data, SEM-EDX data, BET data, TGA data, dynamic mechanical analysis data, permeation data, and sorption data (PDF)

■ AUTHOR INFORMATION

Corresponding Author

Zachary P. Smith − *Department of Chemical Engineering, Massachusetts Institute of Technology, Cambridge, Massachusetts 02139, United States;* orcid.org/0000-0002-9630-5890; Email: zpsmith@mit.edu

https://doi.org/10.1021/acs.chemmater.3c03190
Chem. Mater. 2024, 36, 4275−4290

Authors

Taigyu Joo − *Department of Chemical Engineering, Massachusetts Institute of Technology, Cambridge, Massachusetts 02139, United States*

Tae Hoon Lee − *Department of Chemical Engineering, Massachusetts Institute of Technology, Cambridge, Massachusetts 02139, United States;* orcid.org/0000-0003-0641-0417

Samuel J. Kaser − *Department of Chemistry, Massachusetts Institute of Technology, Cambridge, Massachusetts 02139, United States;* orcid.org/0000-0002-1743-5612

Wan-Ni Wu − *Department of Chemical Engineering, Massachusetts Institute of Technology, Cambridge, Massachusetts 02139, United States;* orcid.org/0000-0001-5520-9248

Sungsool Wi − *National High Magnetic Field Laboratory, Tallahassee, Florida 32304, United States*

Jing Ying Yeo − *Department of Chemical Engineering, Massachusetts Institute of Technology, Cambridge, Massachusetts 02139, United States*

Complete contact information is available at: https://pubs.acs.org/10.1021/acs.chemmater.3c03190

Notes

The authors declare no competing financial interest.

■ ACKNOWLEDGMENTS

This work was supported by the U.S. Department of Energy, Office of Science, Office of Basic Energy Sciences, Separation Science Program under Award Number DE-SC0019087 and the Office of Naval Research (ONR) under Award Numbers N00014-20-1-2418 and N00014-21-1-2666. Additionally, a portion of this work was performed at the National High Magnetic Field Laboratory, which is supported by the National Science Foundation (NSF) Cooperative Agreement Nos. DMR-1644779 and DMR-2128556 and the state of Florida. The authors would like to thank Dr. Holden W. H. Lai and Yifan Wu for their helpful insights related to the proposed crosslinking mechanisms. The authors would like to thank Dr. Kayla R. Storme for her help with the Soxhlet extraction experiment.

■ REFERENCES

(1) International Energy Agency. *CO_2 Emissions in 2022*, 2023. https://www.iea.org/reports/global-energy-review-co2-emissions-in-2021-2.

(2) U.S. Energy Information Administration. *Annual Energy Outlook 2023*, 2023.

(3) Sholl, D. S.; Lively, R. Seven Chemical Separations to Change the World. *Nature* **2016**, *532*, 435−437.

(4) Sanders, D. F.; Smith, Z. P.; Guo, R.; Robeson, L. M.; McGrath, J. E.; Paul, D. R.; Freeman, B. D. Energy-Efficient Polymeric Gas Separation Membranes for a Sustainable Future: A Review. *Polymer* **2013**, *54*, 4729−4761.

(5) Wang, Y.; Ma, X.; Ghanem, B. S.; Alghunaimi, F.; Pinnau, I.; Han, Y. Polymers of Intrinsic Microporosity for Energy-Intensive Membrane-Based Gas Separations. *Mater. Today Nano* **2018**, *3*, 69−95.

(6) Galizia, M.; Chi, W. S.; Smith, Z. P.; Merkel, T. C.; Baker, R. W.; Freeman, B. D. 50th Anniversary Perspective: Polymers and Mixed Matrix Membranes for Gas and Vapor Separation: A Review and Prospective Opportunities. *Macromolecules* **2017**, *50*, 7809−7843.

(7) Robeson, L. M. Correlation of Separation Factor versus Permeability for Polymeric Membranes. *J. Membr. Sci.* **1991**, *62*, 165−185.

(8) Robeson, L. M. The Upper Bound Revisited. *J. Membr. Sci.* **2008**, *320*, 390−400.

(9) Budd, P. M.; McKeown, N. B. Highly Permeable Polymers for Gas Separation Membranes. *Polym. Chem.* **2010**, *1*, 63−68.

(10) Swaidan, R.; Ghanem, B.; Pinnau, I. Fine-Tuned Intrinsically Ultramicroporous Polymers Redefine the Permeability/Selectivity Upper Bounds of Membrane-Based Air and Hydrogen Separations. *ACS Macro Lett.* **2015**, *4* (9), 947−951.

(11) Comesaña-Gándara, B.; Chen, J.; Bezzu, C. G.; Carta, M.; Rose, I.; Ferrari, M. C.; Esposito, E.; Fuoco, A.; Jansen, J. C.; McKeown, N. B. Redefining the Robeson Upper Bounds for CO_2/CH_4 and CO_2/N_2 Separations Using a Series of Ultrapermeable Benzotriptycene-Based Polymers of Intrinsic Microporosity. *Energy Environ. Sci.* **2019**, *12*, 2733−2740.

(12) Budd, P. M.; McKeown, N. B.; Fritsch, D. Free Volume and Intrinsic Microporosity in Polymers. *J. Mater. Chem.* **2005**, *15*, 1977−1986.

(13) Mason, C. R.; Maynard-Atem, L.; Heard, K. W. J.; Satilmis, B.; Budd, P. M.; Friess, K.; Lanč, M.; Bernardo, P.; Clarizia, G.; Jansen, J. C. Enhancement of CO_2 Affinity in a Polymer of Intrinsic Microporosity by Amine Modification. *Macromolecules* **2014**, *47*, 1021−1029.

(14) Mizrahi Rodriguez, K.; Wu, A. X.; Qian, Q.; Han, G.; Lin, S.; Benedetti, F. M.; Lee, H.; Chi, W. S.; Doherty, C. M.; Smith, Z. P. Facile and Time-Efficient Carboxylic Acid Functionalization of PIM-1: Effect on Molecular Packing and Gas Separation Performance. *Macromolecules* **2020**, *53*, 6220−6234.

(15) Du, N.; Robertson, G. P.; Song, J.; Pinnau, I.; Guiver, M. D. High-Performance Carboxylated Polymers of Intrinsic Microporosity (PIMs) with Tunable Gas Transport Properties. *Macromolecules* **2009**, *42* (16), 6038−6043.

(16) Jeon, J. W.; Kim, D. G.; Sohn, E. H.; Yoo, Y.; Kim, Y. S.; Kim, B. G.; Lee, J. C. Highly Carboxylate-Functionalized Polymers of Intrinsic Microporosity for CO_2-Selective Polymer Membranes. *Macromolecules* **2017**, *50* (20), 8019−8027.

(17) Weng, X.; Baez, J. E.; Khiterer, M.; Hoe, M. Y.; Bao, Z.; Shea, K. J. Chiral Polymers of Intrinsic Microporosity: Selective Membrane Permeation of Enantiomers. *Angew. Chem., Int. Ed.* **2015**, *54* (38), 11214−11218.

(18) Mason, C. R.; Maynard-Atem, L.; Al-Harbi, N. M.; Budd, P. M.; Bernardo, P.; Bazzarelli, F.; Clarizia, G.; Jansen, J. C. Polymer of Intrinsic Microporosity Incorporating Thioamide Functionality: Preparation and Gas Transport Properties. *Macromolecules* **2011**, *44* (16), 6471−6479.

(19) Du, N.; Park, H. B.; Robertson, G. P.; Dal-Cin, M. M.; Visser, T.; Scoles, L.; Guiver, M. D. Polymer Nanosieve Membranes for CO_2-Capture Applications. *Nat. Mater.* **2011**, *10* (5), 372−375.

(20) Mizrahi Rodriguez, K.; Lin, S.; Wu, A. X.; Storme, K. R.; Joo, T.; Grosz, A. F.; Roy, N.; Syar, D.; Benedetti, F. M.; Smith, Z. P. Penetrant-Induced Plasticization in Microporous Membranes. *Chem. Soc. Rev.* **2024**, *53*, 2435−3529.

(21) Chen, X.; Fan, Y.; Wu, L.; Zhang, L.; Guan, D.; Ma, C.; Li, N. Ultra-Selective Molecular-Sieving Gas Separation Membranes Enabled by Multi-Covalent-Crosslinking of Microporous Polymer Blends. *Nat. Commun.* **2021**, *12*, 6140.

(22) Du, N.; Dal-Cin, M. M.; Robertson, G. P.; Guiver, M. D. Decarboxylation-Induced Cross-Linking of Polymers of Intrinsic Microporosity (PIMs) for Membrane Gas Separation. *Macromolecules* **2012**, *45* (12), 5134−5139.

(23) Song, Q.; Cao, S.; Pritchard, R. H.; Ghalei, B.; Al-Muhtaseb, S. A.; Terentjev, E. M.; Cheetham, A. K.; Sivaniah, E. Controlled Thermal Oxidative Crosslinking of Polymers of Intrinsic Microporosity towards Tunable Molecular Sieve Membranes. *Nat. Commun.* **2014**, *5*, 4813.

(24) Low, Z. X.; Budd, P. M.; McKeown, N. B.; Patterson, D. A. Gas Permeation Properties, Physical Aging, and Its Mitigation in High Free Volume Glassy Polymers. *Chem. Rev.* **2018**, *118*, 5871−5911.
(25) Lin, S.; Joo, T.; Benedetti, F. M.; Chen, L. C.; Wu, A. X.; Mizrahi Rodriguez, K.; Qian, Q.; Doherty, C. M.; Smith, Z. P. Free Volume Manipulation of a 6FDA-HAB Polyimide Using a Solid-State Protection/Deprotection Strategy. *Polymer* **2021**, *212*, 123121.
(26) Mizrahi Rodriguez, K.; Lin, S.; Wu, A. X.; Han, G.; Teesdale, J. J.; Doherty, C. M.; Smith, Z. P. Leveraging Free Volume Manipulation to Improve the Membrane Separation Performance of Amine-Functionalized PIM-1. *Angew. Chem., Int. Ed.* **2021**, *60*, 6593−6599.
(27) Zhang, C.; Cao, B.; Li, P. Thermal Oxidative Crosslinking of Phenolphthalein-Based Cardo Polyimides with Enhanced Gas Permeability and Selectivity. *J. Membr. Sci.* **2018**, *546*, 90−99.
(28) Zhao, M.; Zhang, C.; Weng, Y.; Li, P. Synergistic Improvement of CO_2/CH_2 Separation Performance of Phenolphthalein-Based Polyimide Membranes by Thermal Decomposition and Thermal-Oxidative Crosslinking. *Polymer* **2022**, *263*, 125528.
(29) Joo, T.; Mizrahi Rodriguez, K.; Lee, H.; Acharya, D. P.; Doherty, C. M.; Smith, Z. P. The Role of Free Volume, Hydrogen Bonds, and Crosslinks on Physical Aging in Polymers of Intrinsic Microporosity (PIMs). *J. Mater. Chem. A* **2023**, *11* (29), 15943−15957.
(30) Fung, B. M.; Khitrin, A. K.; Ermolaev, K. An Improved Broadband Decoupling Sequence for Liquid Crystals and Solids. *J. Magn. Reson.* **2000**, *142* (1), 97−101.
(31) Mizrahi Rodriguez, K.; Benedetti, F. M.; Roy, N.; Wu, A. X.; Smith, Z. P. Sorption-Enhanced Mixed-Gas Transport in Amine Functionalized Polymers of Intrinsic Microporosity (PIMs). *J. Mater. Chem. A* **2021**, *9*, 23631−23642.
(32) Xie, Z.; Dao, B.; Hodgkin, J.; Hoang, M.; Hill, A.; Gray, S. Synthesis and Characterization of Hybrid Organic-Inorganic Materials Based on Sulphonated Polyamideimide and Silica. *J. Polym. Res.* **2011**, *18* (5), 965−973.
(33) Ganesan, M.; Nagaraaj, P. Recent Developments in Dehydration of Primary Amides to Nitriles. *Org. Chem. Front.* **2020**, *7* (22), 3792−3814.
(34) Tunma, S.; Inthanon, K.; Chaiwong, C.; Pumchusak, J.; Wongkham, W.; Boonyawan, D. Improving the Attachment and Proliferation of Umbilical Cord Mesenchymal Stem Cells on Modified Polystyrene by Nitrogen-Containing Plasma. *Cytotechnology* **2013**, *65*, 119−134.
(35) Lyu, H.; Chen, O. I.-F.; Hanikel, N.; Hossain, M. I.; Flaig, R. W.; Pei, X.; Amin, A.; Doherty, M. D.; Impastato, R. K.; Glover, T. G.; Moore, D. R.; Yaghi, O. M. Carbon Dioxide Capture Chemistry of Amino Acid Functionalized Metal-Organic Frameworks in Humid Flue Gas. *J. Am. Chem. Soc.* **2022**, *144* (5), 2387−2396.
(36) Kholodovych, V.; Welsh, W. J. Thermal-Oxidative Stability and Degradation of Polymers. In *Physical Properties of Polymers Handbook*; Mark, J. E., Ed.; Springer: New York, 2007.
(37) Pielichowski, K.; Njuguna, J.; Majka, T. M. *Thermal Degradation of Polymeric Materials*, 2nd ed.; Elsevier Science: Amsterdam, 2022.
(38) Nakatani, H.; Suzuki, S.; Tanaka, T.; Terano, M. New Kinetic Aspects on the Mechanism of Thermal Oxidative Degradation of Polypropylenes with Various Tacticities. *Polymer* **2005**, *46* (26), 12366−12371.
(39) Hawkins, W. L. Thermal and Oxidative Degradation of Polymers. *Polym. Eng. Sci.* **1964**, *4* (3), 187−192.
(40) Peterson, J. D.; Vyazovkin, S.; Wight, C. A. Kinetics of the Thermal and Thermo-Oxidative Degradation of Polystyrene, Polyethylene and Poly(Propylene). *Macromol. Chem. Phys.* **2001**, *202*, 775−784.
(41) Budd, P. M.; Elabas, E. S.; Ghanem, B. S.; Makhseed, S.; McKeown, N. B.; Msayib, K. J.; Tattershall, C. E.; Wang, D. Solution-Processed, Organophilic Membrane Derived from a Polymer of Intrinsic Microporosity. *Adv. Mater.* **2004**, *16*, 456−459.
(42) Sayari, A.; Heydari-Gorji, A.; Yang, Y. CO_2-Induced Degradation of Amine-Containing Adsorbents: Reaction Products and Pathways. *J. Am. Chem. Soc.* **2012**, *134* (33), 13834−13842.
(43) Dong, W.; Gijsman, P. Influence of Temperature on the Thermo-Oxidative Degradation of Polyamide 6 Films. *Polym. Degrad. Stab.* **2010**, *95* (6), 1054−1062.
(44) Gonçalves, E. S.; Poulsen, L.; Ogilby, P. R. Mechanism of the Temperature-Dependent Degradation of Polyamide 66 Films Exposed to Water. *Polym. Degrad. Stab.* **2007**, *92* (11), 1977−1985.
(45) Okamba-Diogo, O.; Richaud, E.; Verdu, J.; Fernagut, F.; Guilment, J.; Fayolle, B. Molecular and Macromolecular Structure Changes in Polyamide 11 during Thermal Oxidation. *Polym. Degrad. Stab.* **2014**, *108*, 123−132.
(46) Zhang, Y.; Cheng, Y.; Cai, H.; He, S.; Shan, Q.; Zhao, H.; Chen, Y.; Wang, B. Catalyst-Free Aerobic Oxidation of Aldehydes into Acids in Water under Mild Conditions. *Green Chem.* **2017**, *19* (23), 5708−5713.
(47) Carneiro, J. S. A.; Innocenti, G.; Moon, H. J.; Guta, Y.; Proaño, L.; Sievers, C.; Sakwa-Novak, M. A.; Ping, E. W.; Jones, C. W. Insights into the Oxidative Degradation Mechanism of Solid Amine Sorbents for CO_2 Capture from Air: Roles of Atmospheric Water. *Angew. Chem., Int. Ed.* **2023**, *62* (24), No. e202302887.
(48) Delebecq, E.; Pascault, J. P.; Boutevin, B.; Ganachaud, F. On the Versatility of Urethane/Urea Bonds: Reversibility, Blocked Isocyanate, and Non-Isocyanate Polyurethane. *Chem. Rev.* **2013**, *113* (1), 80−118.
(49) Beckwith, A. L. J. Synthesis of Amides. In *The chemistry of amides*; Zabicky, J., Ed.; John Wiley & Sons Ltd: London, 1970; pp 73−186.
(50) Sorenson, W. R. Reaction of an Isocyanate and a Carboxylic Acid in Dimethyl Sulfoxide. *J. Org. Chem.* **1959**, *24* (7), 978−980.
(51) Gazizov, A. S.; Smolobochkin, A. V.; Rizbayeva, T. S.; Vatsadze, S. Z.; Burilov, A. R.; Sinyashin, O. G.; Alabugin, I. V. Stereoelectronic Deprotection of Nitrogen": Recovering Nucleophilicity with a Conformational Change. *J. Org. Chem.* **2023**, *88* (11), 6868−6877.
(52) Ying, H.; Zhang, Y.; Cheng, J. Dynamic Urea Bond for the Design of Reversible and Self-Healing Polymers. *Nat. Commun.* **2014**, *5*, 3218.
(53) Mizrahi Rodriguez, K.; Wu, W. N.; Alebrahim, T.; Cao, Y.; Freeman, B. D.; Harrigan, D.; Jhalaria, M.; Kratochvil, A.; Kumar, S.; Lee, W. H.; Lee, Y. M.; Lin, H.; Richardson, J. M.; Song, Q.; Sundell, B.; Thür, R.; Vankelecom, I.; Wang, A.; Wang, L.; Wiscount, C.; Smith, Z. P. Multi-Lab Study on the Pure-Gas Permeation of Commercial Polysulfone (PSf) Membranes: Measurement Standards and Best Practices. *J. Membr. Sci.* **2022**, *659*, 120746.
(54) Lin, R.-B.; Li, L.; Zhou, H.-L.; Wu, H.; He, C.; Li, S.; Krishna, R.; Li, J.; Zhou, W.; Chen, B. Molecular Sieving of Ethylene from Ethane Using a Rigid Metal-Organic Framework. *Nat. Mater.* **2018**, *17* (12), 1128−1133.
(55) McCaig, M. S.; Paul, D. R. Effect of UV Crosslinking and Physical Aging on the Gas Permeability of Thin Glassy Polyarylate Films. *Polymer* **1999**, *40*, 7209−7225.
(56) Vanherck, K.; Koeckelberghs, G.; Vankelecom, I. F. J. Crosslinking Polyimides for Membrane Applications: A Review. *Prog. Polym. Sci.* **2013**, *38* (6), 874−896.
(57) Rungta, M.; Zhang, C.; Koros, W. J.; Xu, L. Membrane-Based Ethylene/Ethane Separation: The Upper Bound and Beyond. *AIChE J.* **2013**, *59* (9), 3475−3489.
(58) Rowe, B. W.; Freeman, B. D.; Paul, D. R. Physical Aging of Membranes for Gas Separations. In *Membrane Engineering for the Treatment of Gases*; Drioli, E., Barbieri, G., Eds.; Royal Society of Chemistry Books: Cambridge, 2011; Vol. *1*, pp 58−83.
(59) Scholes, C. A.; Stevens, G. W.; Kentish, S. E. Membrane Gas Separation Applications in Natural Gas Processing. *Fuel* **2012**, *96*, 15−28.
(60) Vieth, W. R.; Howell, J. M.; Hsieh, J. H. Dual Sorption Theory. *J. Membr. Sci.* **1976**, *1*, 177−220.

https://doi.org/10.1021/acs.chemmater.3c03190
Chem. Mater. 2024, 36, 4275−4290

(61) Borden, W. T.; Hoffmann, R.; Stuyver, T.; Chen, B. Dioxygen: What Makes This Triplet Diradical Kinetically Persistent? *J. Am. Chem. Soc.* **2017**, *139* (26), 9010−9018.
(62) Guo, S.; Yeo, J. Y.; Benedetti, F. M.; Syar, D.; Swager, T. M.; Smith, Z. P. A Microporous Poly(Arylene Ether) Platform for Membrane-Based Gas Separation. *Angew. Chem., Int. Ed.* **2024**, *63* (8), No. e202315611.
(63) Li, F. Y.; Xiao, Y.; Chung, T. S.; Kawi, S. High-Performance Thermally Self-Cross-Linked Polymer of Intrinsic Microporosity (PIM-1) Membranes for Energy Development. *Macromolecules* **2012**, *45*, 1427−1437.
(64) Khan, M. M.; Bengtson, G.; Shishatskiy, S.; Gacal, B. N.; Mushfequr Rahman, M.; Neumann, S.; Filiz, V.; Abetz, V. Cross-Linking of Polymer of Intrinsic Microporosity (PIM-1) via Nitrene Reaction and Its Effect on Gas Transport Property. *Eur. Polym. J.* **2013**, *49* (12), 4157−4166.
(65) Du, N.; Cin, M. M. D.; Pinnau, I.; Nicalek, A.; Robertson, G. P.; Guiver, M. D. Azide-Based Cross-Linking of Polymers of Intrinsic Microporosity (PIMs) for Condensable Gas Separation. *Macromol. Rapid Commun.* **2011**, *32* (8), 631−636.
(66) Sun, Y.; Zhang, J.; Li, H.; Fan, F.; Zhao, Q.; He, G.; Ma, C. Ester-Crosslinked Polymers of Intrinsic Microporosity Membranes with Enhanced Plasticization Resistance for CO_2 Separation. *Sep. Purif. Technol.* **2023**, *314*, 123623.
(67) Wang, L.; Guo, X.; Zhang, F.; Li, N. Blending and in Situ Thermally Crosslinking of Dual Rigid Polymers for Anti-Plasticized Gas Separation Membranes. *J. Membr. Sci.* **2021**, *638*, 119668.
(68) Chen, X.; Zhang, Z.; Wu, L.; Liu, X.; Xu, S.; Efome, J. E.; Zhang, X.; Li, N. Polymers of Intrinsic Microporosity Having Bulky Substitutes and Cross-Linking for Gas Separation Membranes. *ACS Appl. Polym. Mater.* **2020**, *2* (2), 987−995.
(69) Zhou, S.; Sun, Y.; Xue, B.; Li, S.; Zheng, J.; Zhang, S. Controlled Superacid-Catalyzed Self-Cross-Linked Polymer of Intrinsic Microporosity for High-Performance CO_2 Separation. *Macromolecules* **2020**, *53* (18), 7988−7996.
(70) Neumann, S.; Bengtson, G.; Meis, D.; Filiz, V. Thermal Cross Linking of Novel Azide Modified Polymers of Intrinsic Microporosity—Effect of Distribution and the Gas Separation Performance. *Polymers* **2019**, *11* (8), 1241.
(71) Huang, M.; Lu, K.; Wang, Z.; Bi, X.; Zhang, Y.; Jin, J. Thermally Cross-Linked Amidoxime-Functionalized Polymers of Intrinsic Microporosity Membranes for Highly Selective Hydrogen Separation. *ACS Sustain. Chem. Eng.* **2021**, *9* (28), 9426−9435.
(72) Zhang, T.; Deng, L.; Li, P. Decarboxylation Cross-Linking of Triptycene-Based Tröger's Base Polymers for Gas Separation. *Ind. Eng. Chem. Res.* **2020**, *59* (41), 18640−18648.
(73) Zhang, C.; Fu, L.; Tian, Z.; Cao, B.; Li, P. Post-Crosslinking of Triptycene-Based Tröger's Base Polymers with Enhanced Natural Gas Separation Performance. *J. Membr. Sci.* **2018**, *556* (15), 277−284.

https://doi.org/10.1021/acs.chemmater.3c03190
Chem. Mater. 2024, 36, 4275−4290